Local Excitation of Kagome Spin Ice Magnetism Seen by Scanning Tunneling Microscopy

Hanbin Deng[1,*] Tianyu Yang,[1,*] Guowei Liu,[1,*] Lu Liu,[1,*] Lingxiao Zhao,[1,2,*] Wu Wang,[1] Tiantian Li,[1,3] Wei Song,[1] Titus Neupert,[4] Xiang-Rui Liu,[1,5] Jifeng Shao,[5] Y. Y. Zhao,[2] Nan Xu,[6] Hao Deng,[7] Li Huang,[1] Yue Zhao,[1,5] Liyuan Zhang,[1,2] Jia-Wei Mei,[1,5] Liusuo Wu,[1,8] Jiaqing He,[1] Qihang Liu,[1,5,8,†] Chang Liu,[1,5] and Jia-Xin Yin[1,2,‡]

[1]*Department of Physics, Southern University of Science and Technology, Shenzhen, China*
[2]*Quantum Science Center of Guangdong-Hong Kong-Macao Greater Bay Area (Guangdong), Shenzhen, China*
[3]*Shenzhen Key Laboratory of Advanced Quantum Functional Materials and Devices,*
Southern University of Science and Technology, Shenzhen, China
[4]*Department of Physics, University of Zurich, Winterthurerstrasse, Zurich, Switzerland*
[5]*Shenzhen Institute for Quantum Science and Engineering, Southern University of Science and Technology,*
Shenzhen, Guangdong, China
[6]*Institute for Advanced Studies, Wuhan University, Wuhan 430072, China*
[7]*School of Physical Science and Technology, ShanghaiTech University, Shanghai 201210, China*
[8]*Guangdong Provincial Key Laboratory of Computational Science and Material Design,*
Southern University of Science and Technology, Shenzhen, China

The kagome spin ice can host frustrated magnetic excitations by flipping its local spin. Under an inelastic tunneling condition, the tip in a scanning tunneling microscope can flip the local spin, and we apply this technique to kagome metal HoAgGe with a long-range ordered spin ice ground state. Away from defects, we discover a pair of pronounced dips in the local tunneling spectrum at symmetrical bias voltages with negative intensity values, serving as a striking inelastic tunneling signal. This signal disappears above the spin ice formation temperature and has a dependence on the magnetic fields, demonstrating its intimate relation with the spin ice magnetism. We provide a two-level spin-flip model to explain the tunneling dips considering the spin ice magnetism under spin-orbit coupling. Our results uncover a local emergent excitation of spin ice magnetism in a kagome metal, suggesting that local electrical field induced spin flip climbs over a barrier caused by spin-orbital locking.

A kagome lattice is made of corner-sharing triangles. Based on its special geometry, the kagome lattice can host frustrated magnetic or electronic structures, including quantum spin liquids [1], spin ices [2,3], and flat electronic bands [4,5]. Recent years have witnessed substantial advances in exploring the emergent physics of metallic kagome quantum materials using electronic structure methods [4,5], highlighting the interplay between geometry, topology, correlation, and spin. However, the quantum spin liquid and spin ice phase in the kagome lattice are largely unexplored by advanced electronic structure methods. In this Letter, we advance this research frontier by detecting pronounced tunneling conductance dips in kagome spin ice HoAgGe, serving as the signature of local spin-flip that is crucial for harnessing frustrated spin ice excitations.

In spin ice materials, the local magnetic spins respect "ice rules" similar to the electrical dipoles in water ice [2,4,6–13]. The spin ice is typically found in quantum materials with three-dimensional pyrochlore lattices, and has been recently discovered in a kagome metal HoAgGe [13]. In a kagome spin ice, the ice rule requires 2-in-1-out or 2-out-1-in spin configurations in each triangle [Fig. 1(a)]. Upon lowering the temperature, it is believed that spins first form a short-range ice order and then a long-range ice order. Intriguingly, when locally breaking the ice rule by flipping a certain spin, spin configurations with three in or three out can emerge, in analogy to the magnetic monopoles predicted by Dirac [14]. Creating spin excitations in a controlled and local manner can open new avenues for spin ice research.

HoAgGe consists of distorted Ho^{3+} kagome lattices with layer stacking [Fig. 1(b)], where the strong local easy-axis anisotropy together with the ferromagnetic nearest-neighbor coupling of the Ho^{3+} moments lead to "1-in-2-out" or "2-in-1-out" ice rules on the kagome lattice [Fig. 1(c)] [13]. The atomic structure of HoAgGe single crystal [Fig. 1(d)] is demonstrated by the high angle annular dark-field-scanning transmission electron microscopy in an aberration-corrected transmission electron microscopy, as shown in Fig. 1(e). The high-resolution image and corresponding elemental maps clearly show the Ho kagome structure in the *a-b* plane with the well-identified Ho, Ag, and Ge atoms. Its short-range spin ice order occurs at around 20 K, while its long-range spin ice
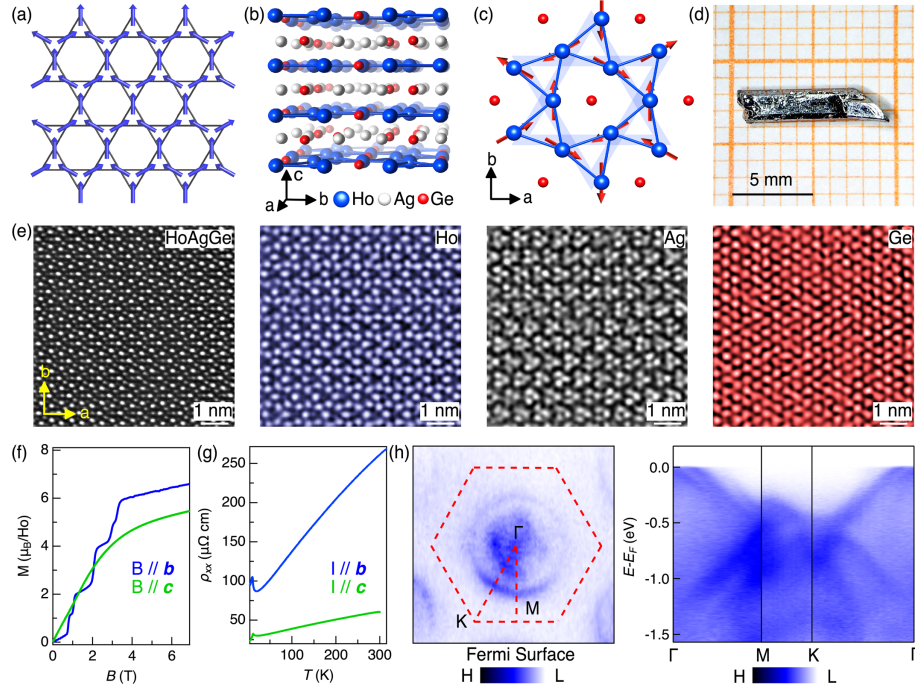
FIG. 1. Coexistence of local moment and itinerant electrons in kagome spin ice HoAgGe. (a) Schematic for a kagome spin ice. (b) Crystal structure of HoAgGe showing layered structure. (c) The distorted Ho kagome lattice with spins following the ice rule, the shaded lines show a perfect kagome lattice. (d) Image of a HoAgGe single crystal with its c axis along the horizontal direction. (e) High-angle annular dark-field-scanning transmission electron microscopy image (left) and corresponding energy-dispersive spectrometry elemental maps (right), imaged along the c axis. (f) Low-temperature magnetization curves measured at 2 K, where the in-plane magnetization curve shows fractional field-induced transitions. (g) Resistivity curve showing metallic behavior of HoAgGe. (h) Fermi surfaces (left) and band dispersions along the high symmetry lines (right) detected by angle-resolved photoemission at 8 K.

order occurs at 11.6 K [13]. In the spin ice state, magnetization versus external magnetic fields parallel to the kagome plane exhibits a series of plateaus [Fig. 1(f)], and the corresponding field-induced phases detected by neutron scattering are all consistent with the spin ice rule [13]. Magnetization along the c axis, on the other hand, shows a gradual increment with field strength [Fig. 1(f)] that is consistent with a ferromagnetic canting of the spins toward the c axis [13]. The temperature-dependent resistivity data [Fig. 1(g)] shows a peak feature near the spin ice transition and demonstrates metallic behavior. Consistently, our angle-resolved photoemission spectroscopy characterization of this material at the spin ice state ($T = 8$ K) reveals both Fermi surfaces and multiple dispersive bands at the Fermi level [Fig. 1(h)]. The magnetization plateaus and dispersive bands together demonstrate the coexistence of local moments and itinerant electrons. This situation allows us to use the electronic tunneling method to introduce spin excitations that we further explore.

Compared to other techniques, scanning tunneling microscope can flip the spin of a single atom through inelastic tunneling [15–21], and is highly desirable to be applied to study kagome spin ice [Fig. 2(a)]. Above a threshold tunneling bias voltage, electrons can transfer energy to the spin-flip excitations. In this Letter, we explore this frontier in kagome spin ice HoAgGe. Owing to the strong interlayer bonding, it is extremely rare to obtain a

flat atomic surface by cryogenic cleaving, which severely challenges its scanning tunneling microscopy study. Therefore, we have to cleave more than 50 crystals and scan extensively for each cleaved crystal to find the atomic flat surface with unit-cell step heights [Figs. 2(b) and 2(c)]. The surface exhibits a hexagonal lattice with its lattice constant consistent with that of the crystal [Fig. 2(d)]. In the crystal structure, only Ge atoms in the HoGe layer form a hexagonal lattice. Thus, we identify this surface as HoGe surface termination. At low-temperature $T = 0.3$ K, we measure the differential conductance spectrum in the clean lattice region and detect a pair of pronounced dips located at $E_d = \pm 107$ meV [Fig. 2(e)], with corresponding kinks in the tunneling current data [Fig. 2(f)]. Such dips are the most pronounced features in the data and extra tiny spectral dips (not reaching to negative value) and bumps are currently not well understood. The energy locations of this pair of dips are symmetric, and their corresponding differential conductance values are strongly negative. These two features indicate the dips are from inelastic tunneling rather than from the density of states of the band structure, as also confirmed by the absence of such a feature around -0.1 eV in our photoemission data in Fig. 1(h). These titanic spectral features are different from the mild step features for inelastic tunneling of spin flip of an isolated magnetic atom [15–19]. To understand their origin, we
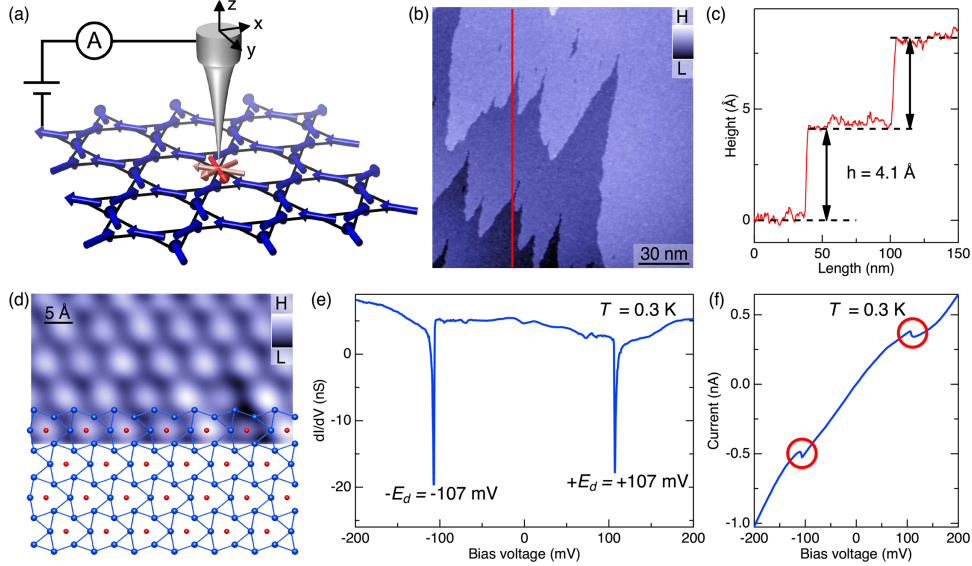
FIG. 2. Pronounced tunneling dips in kagome spin ice HoAgGe. (a) Schematic for scanning tip probe induced local spin-flip in a kagome spin ice. (b) Topographic image for a large field of view showing atomic flat cleaving surfaces with unit-cell height steps. (c) Height profile along the red line drawn in (b), showing atomic step height of 4.1 Å that is consistent with the unit cell height. (d) A close-up image of the topographic image (up) whose lattice symmetry is consistent with the HoGe atomic layer (down). (e) Differential conductance spectrum on the clean region of HoGe surface showing a pair of pronounced electronic dips occurring at $E_d = \pm 107$ mV. (f) The corresponding kinks in the tunneling current spectrum.

systematically examine their spatial, temperature, and magnetic responses in Fig. 3.

We perform a spectroscopic map at the dip energy for a large area in Figs. 3(a) and 3(b). The spectroscopic map data are inhomogeneous, and the low-intensity parts of the map correspond to the emergence of dips, as further supported by representative differential conductance spectra along a line cut [Fig. 3(d)]. Owing to the strong interlayer bonding, the cleavage leaves vacancies and adatoms as surface defects, and we find that the dips are generically away from these defects as illustrated in Fig. 3(c), where we mark the positions of both the impurities and dips. Hence the local dip feature can be an intrinsic feature of the clean lattice rather than from impurities, and the inhomogeneity is largely caused by cleavage-induced surface defects that have a long-range suppression of the dip feature. When we raise the temperature, we find that while the dip energy does not change, the dip becomes progressively shallow, and eventually disappears above 20 K [Fig. 3(e)]. It is close to the short-range spin ice order transition temperature, as evidenced by the differential heat capacity [reproduced in the inset of Fig. 3(e)]. At the defect-free region, we further find that the external magnetic field also does not change dip energy [Fig. 3(f)], but only affect its depth. An in-plane magnetization (the sample riches the 1/3 magnetization plateau with $B = 1.5$ T applied along the b axis [13,22]) enhances the depth of the dip, while an out-of-plane magnetization (the sample riches the magnetization plateau with $B = 6$ T applied along the c axis) suppresses the depth

of the dip. We note that after applying the magnetic field or varying the temperature, we relax the system and relocate our tip to the same atomic position to take the differential spectrum. We clarify that these data are representative data rather than statistical data. The spatial, temperature, and magnetic field responses thus support the intimate relation between the pronounced tunneling dip and spin ice magnetism of the kagome lattice, and we discuss its possible microscopic origin.

In terms of magnetic excitations, the common inelastic tunneling signal can result from the spin-flip process [15–19]. The spin-flip energy Δ_S is related to the magnetic exchange interaction on the order of 1–10 meV, inferred from the short-range spin ice transition temperature of 20 K. As Ho carries heavy $4f$ orbitals with a large spin-orbit coupling, we need to consider the orbital flip locked to the spin-flip. Since there is no apparent orbital ordering from transport, the finial orbital flipped state would not alter the dip energy too much; however, the intermediate orthogonal orbital configuration can be at much higher energy in the anisotropic crystal field, causing an energy barrier Δ_O. Therefore, the spin-flip process here can be described by a two-level system with a small spin energy difference of Δ_S and a large orbital barrier Δ_O [Fig. 4(a)]. Notably, a similar vibrationally induced two-level picture has been pointed out to explain spikes in differential conductance in molecular junctions [23]. This model further assumes different tunneling conductance values for the two energy levels, and it can naturally produce a pair of tunneling dips at symmetrical energies, as illustrated by our simulations
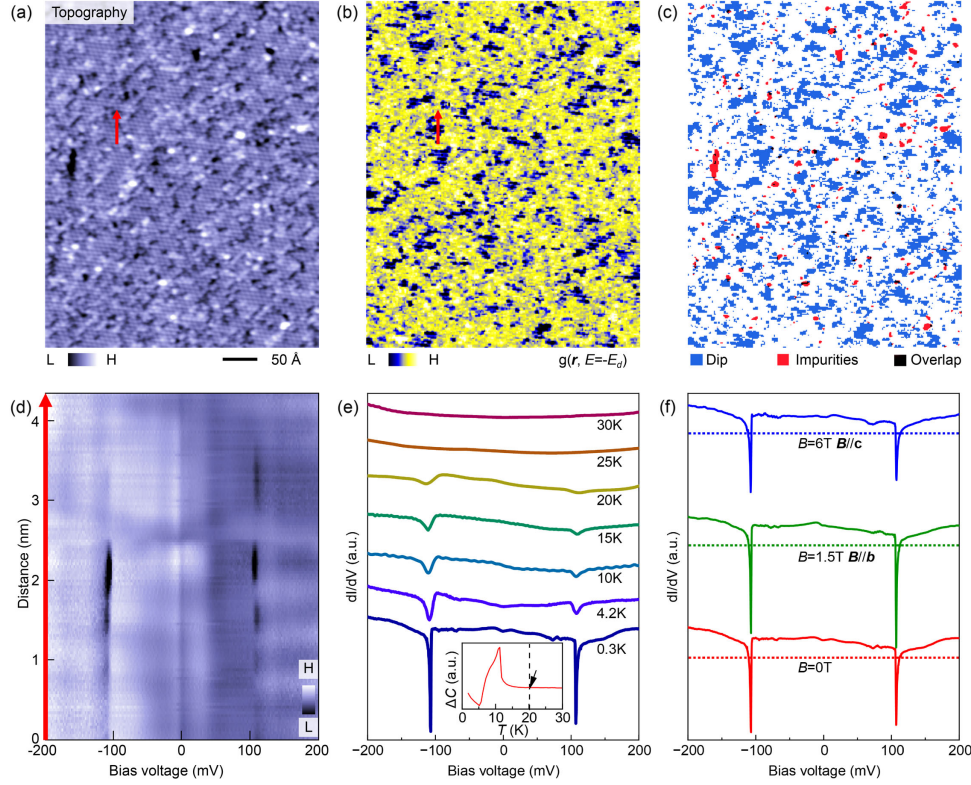
FIG. 3. Spatial, temperature, and magnetic field dependence of the tunneling dips. (a) Topographic image of a large cleavage surface. The surface contains adatoms and vacancies as impurities caused by cleavage. (b) Differential conductance map $g(r, E)$ at the dip energy, showing inhomogeneity. (c) Anticorrelation between the dips and impurities. We find the dips are generally away from the impurities, indicating that dips are intrinsic features of the clean lattice. (d) Intensity plot of a series of differential conductance spectra along the red line drawn in (a) and (b), showing the spatial inhomogeneity of dips at $E_d = \pm 107$ meV. (e) Temperature dependence of the dips at a fixed position, showing its disappearance above 20 K. The inset shows the differential heat capacity reproduced from Ref. [13], where the short-range spin ice formation temperature is estimated to be around 20 K. (f) Magnetic field dependence of the dip at a fixed position. An in-plane magnetization (the sample riches the $1/3$ magnetization plateau with $B = 1.5$ T applied along the b axis) enhances the depth of the dip, while an out-of-plane magnetization (the sample riches the magnetization plateau with $B = 6$ T applied along the c axis) suppresses the depth of the dip. The dashed lines mark the respective zero value.

[Fig. 4(b)], which strongly supports our two-level interpretation of the data.

To demonstrate the two-level spin-flip scenario, we present quantitative calculations of the two essential energy levels, i.e., Δ_S and Δ_O. Based on the estimation [13] of local exchange interactions J from the magnetization data, we calculate the lowest spin-flip energy $\Delta_S = 2J_2S^2 = 2$ meV as shown in Fig. 4(c), where $J_2 = 0.23$ meV and $S = 2$. The calculated Δ_S aligns well, in terms of the order of magnitude, with the extracted values presented in Fig. 4(e). To estimate the energy barrier of spin-flip Δ_O, we calculate the crystal electric field (CEF) of Ho^{3+} ion on the cleavage HoGe surface, where the surrounding ligands are Ge^{4-} and Ho^{3+} ions (note that it differs from the bulk CEF). The $|J = 8, J_z\rangle$ multiplet ($S = 2, L = 6$) of the Ho^{3+} ion, under the C_{2v} site symmetry of Ho^{3+} ion, splits into 17 singlets [24]. We find that the ground state of Ho^{3+} ion manifests Ising anisotropy, with its local axis lying in the ab plane, aligning with the spin ice state in HoAgGe.

Moreover, we note that CEF excitations would be accompanied by spin-flip. In particular, the highest CEF level, with its magnetic easy axis perpendicular to that of the ground state, contributes to the energy barrier during the spin-flip process. This barrier is estimated to be $\Delta_O = 102$ meV [Fig. 4(d)], yielding good quantitative agreement with the observed dips at $E_d = \pm 107$ meV.

In addition, as illustrated in Fig. 4(e), the two-level spin-flip model well reproduces the dependence of tunneling dips on the external magnetic field. Notably, the external field mainly changes the spin-flip energy Δ_S. The 1.5 T in-plane field alone would not break the in-plane ice rule (at the $1/3$ magnetization plateau), but can assist spin-flip of inelastic tunneling for half of the spins in the system by introducing Zeeman energy. Thus, it reduces the minimum spin-flip energy Δ_S of the total spin system. As for the out-of-plane magnetic field, it will polarize spins to tilt toward the c axis. Consequently, the Δ_S now has an additional energy contribution from the nearest magnetic exchange J_1, leading to a moderate increase in its value.
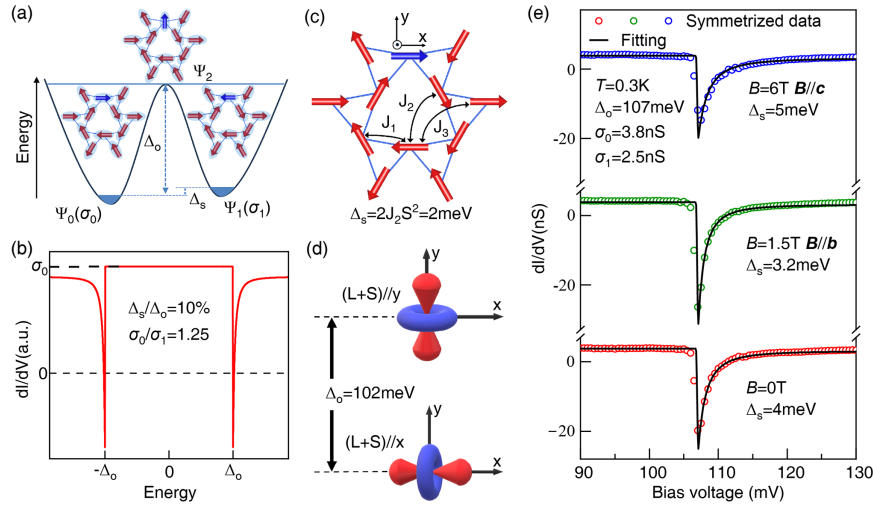
FIG. 4. Two-level spin-flip model for tunneling dips. (a) Schematic for two-level spin-flip process. In this model, Ψ_0 is the kagome spin ice ground state with a differential conductance σ_0, Ψ_1 corresponds to the spin-flipped state with a differential conductance σ_1, and $\Delta_S = 1$–10 meV is their spin energy difference. Ψ_2 is the intermediate state with orthogonal spin and orbital configurations, and it has a large energy difference $\Delta_O \sim 0.1$ eV from the anisotropic crystal electrical field. The three inset figures illustrate three different states by flipping a local spin in the distorted kagome lattice. (b) A typical simulation result of the two-level spin-flip model showing a pair of tunneling dips. (c) Illustration of three superexchange interactions $J_{1,2,3}$ in the distorted kagome lattice. The minimum spin flip energy is calculated to be 2 meV based on the estimated J values from the magnetization data [13]. (d) Calculated orbital barrier energy $\Delta_O = 102$ meV from the largest crystal electric field energy level. (e) Fitting results of the magnetic field dependent tunneling dips by the two-level spin-flip model. The experimental data are symmetrized with respect to zero energy.

In summary, we extend the study of kagome materials with electronic structure methods to a kagome spin ice material, and detect pronounced tunneling dips as the signature of local spin flip. We show that the local spin-flip physics in a magnetic lattice through inelastic tunneling is different from the case of a single magnetic atom, and is well described by a two-level model involving a crystal field barrier. Our interpretation of the data leads us to conclude that effective magnetic monopoles can be pairwise created via inelastic tunneling using a scanning tunneling microscope tip. It is also meaningful to further explore the pronounced dip signal with a spin-polarized tunneling tip [30], since the spin-polarized tunneling has been achieved in other kagome materials [31–33]. Therefore, our exploration of the local spin-flip process in a spin ice system provides an initial step toward harnessing its unusual spin excitations including the magnetic monopoles. The gigantic tunneling signal in a kagome spin ice with classical spins opens up new research opportunities that encourage us to further explore the kagome spin liquid with electronic structure tools.

[1] C. Broholm, R. J. Cava, S. A. Kivelson, D. G. Nocera, M. R. Norman, and T. Senthil, Science **367**, eaay0668 (2020).

[2] C. Nisoli, R. Moessner, and P. Schiffer, Rev. Mod. Phys. **85**, 1473 (2013).

[3] S. H. Skjærvø, C. H. Marrows, R. L. Stamps, and L. J. Heyderman, Nat. Rev. Phys. **2**, 13 (2020).

[4] J. X. Yin, B. Lian, and M. Z. Hasan, Nature (London) **612**, 647 (2022).

[5] Y. Wang, H. Wu, G. T. McCandless, J. Y. Chan, and M. N. Ali, Nat. Rev. Phys. **5**, 635 (2023).

[6] L. Pauling, J. Am. Chem. Soc. **57**, 2680 (1935).

[7] M. J. Harris, S. T. Bramwell, D. F. McMorrow, T. Zeiske, and K. W. Godfrey, Phys. Rev. Lett. **79**, 2554 (1997).

[8] A. P. Ramirez, A. Hayashi, R. J. Cava, R. Siddharthan, and B. S. Shastry, Nature (London) **399**, 333 (1999).

[9] S. T. Bramwell and M. J. P. Gingras, Science **294**, 1495 (2001).

[10] C. Castelnovo, R. Moessner, and S. L. Sondhi, Nature (London) **451**, 42 (2008).

[11] D. J. P. Morris *et al.*, Science **326**, 411 (2009).

[12] T. Fennell, P. P. Deen, A. R. Wildes, K. Schmalzl, D. Prabhakaran, A. T. Boothroyd, R. J. Aldus, D. F. McMorrow, and S. T. Bramwell, Science **326**, 415 (2009).

[13] K. Zhao, H. Deng, H. Chen, K. A. Ross, V. Petříček, G. Günther, M. Russina, V. Hutanu, and P. Gegenwart, Science **367**, 1218 (2020).

[14] P. A. M. Dirac, Proc. R. Soc. A **133**, 60 (1931).

[15] A. J. Heinrich, J. A. Gupta, C. P. Lutz, and D. M. Eigler, Science **306**, 466 (2004).

[16] C. F. Hirjibehedin, C.-Y. Lin, A. F. Otte, M. Ternes, C. P. Lutz, B. A. Jones, and A. J. Heinrich, Science **317**, 1199 (2007).

[17] X. Chen, Y.-S. Fu, S.-H. Ji, T. Zhang, P. Cheng, X.-C. Ma, X.-L. Zou, W.-H. Duan, J.-F. Jia, and Q.-K. Xue, Phys. Rev. Lett. **101**, 197208 (2008).

[18] T. Miyamachi *et al.*, Nature (London) **503**, 242 (2013).

[19] M. Ternes, New J. Phys. **17**, 063016 (2015).

[20] T. Balashov, A. F. Takács, W. Wulfhekel, and J. Kirschner, Phys. Rev. Lett. **97**, 187201 (2006).

[21] Somesh Chandra Ganguli, Markus Aapro, Shawulienu Kezilebieke, Mohammad Amini, Jose L. Lado, and Peter Liljeroth, Nano Lett. **23**, 3412 (2023).

[22] K. Zhao, Y. Tokiwa, H. Chen, and P Gegenwart, Nat. Phys. **20**, 442 (2024).

[23] W. H. A. Thijssen, D. Djukic, A. F. Otte, R. H. Bremmer, and J. M. van Ruitenbeek, Phys. Rev. Lett. **97**, 226806 (2006).

[24] See Supplemental Material at http://link.aps.org/supplemental/10.1103/PhysRevLett.133.046503 for the calculation of the surface crystal electric field, which includes Refs. [25–29].

[25] G. Kresse and J. Furthmuller, Phys. Rev. B **54**, 11169 (1996).

[26] J. P. Perdew, K. Burke, and M. Ernzerhof, Phys. Rev. Lett. **78**, 1396(E) (1997).

[27] D. J. Newman and B. Ng, *Crystal Field Handbook* (Cambridge University Press, Cambridge, England, 2000).

[28] A. Scheie, J. Appl. Crystallogr. **54**, 356 (2021).

[29] S. Watanabe, Proc. Natl. Acad. Sci. U.S.A. **118**, e2112202118 (2021).

[30] R. Wiesendanger, Rev. Mod. Phys. **81**, 1495 (2009).

[31] J.-X. Yin *et al.*, Nat. Commun. **11**, 4415 (2020).

[32] Y. Xing *et al.*, Nat. Commun. **11**, 5613 (2020).

[33] J.-X. Yin *et al.*, Phys. Rev. Lett. **129**, 166401 (2022).